Structure
Article

Structural Analysis of the DAP5 MIF4G Domain and Its Interaction with eIF4A

Geneviève Virgili,[1,2,5] Filipp Frank,[1,2,3,5] Kateryna Feoktistova,[4] Maxime Sawicki,[1,2] Nahum Sonenberg,[1,3] Christopher S. Fraser,[4] and Bhushan Nagar[1,2,*]
[1]Department of Biochemistry
[2]Groupe de Recherche Axé sur la Structure des Protéines
[3]Goodman Cancer Center
McGill University, Montreal, QC H3G 0B1, Canada
[4]Department of Molecular and Cellular Biology, College of Biological Sciences, University of California, Davis, Davis, CA 95616, USA
[5]These authors contributed equally to this work
*Correspondence: bhushan.nagar@mcgill.ca
http://dx.doi.org/10.1016/j.str.2013.01.015

SUMMARY

Death-associated protein 5 (DAP5/p97) is a homolog of the eukaryotic initiation factor 4G (eIF4G) that promotes the IRES-driven translation of multiple cellular mRNAs. Central to its function is the middle domain (MIF4G), which recruits the RNA helicase eIF4A. The middle domain of eIF4G consists of tandem HEAT repeats that coalesce to form a solenoid-type structure. Here, we report the crystal structure of the DAP5 MIF4G domain. Its overall fold is very similar to that of eIF4G; however, significant conformational variations impart distinct surface properties that could explain the observed differences in IRES binding between the two proteins. Interestingly, quantitative analysis of the DAP5-eIF4A interaction using isothermal titration calorimetry reveals a 10-fold lower affinity than with the eIF4G-eIF4A interaction that appears to affect their ability to stimulate eIF4A RNA unwinding activity in vitro. This difference in stability of the complex may have functional implications in selecting the mode of translation initiation.

INTRODUCTION

Translation initiation is the rate-limiting step of protein synthesis and involves assembly of the ribosome on the mRNA followed by recognition of the start codon. Initiation can be carried out in two different ways: the canonical mode of translation initiation is cap-dependent and proceeds by assembly of the eIF4F complex on the mRNA 5′ m^7GpppX cap (where X is any nucleotide) structure and subsequent formation of the preinitiation complex containing the 40S ribosomal subunit (Sonenberg and Hinnebusch, 2009). An alternative mode of translation initiation is cap-independent and involves access of the ribosome to the mRNA via an internal ribosomal entry site (IRES) typically found in the 5′ untranslated region (5′ UTR) (Holcik and Sonenberg, 2005). The IRES recruits the ribosome directly without the need for the mRNA cap or eIF4E.

The eIF4F complex consists of the cap-binding protein eIF4E, the scaffolding protein eIF4G, and an ATP-dependent RNA helicase eIF4A, whose RNA duplex unwinding and ATP hydrolysis activities are coupled and stimulated by eIF4B and eIF4G (Özeş et al., 2011). eIF4G is a large 175 kDa protein with interaction sites for its binding partners spread over multiple domains (Figure 1A). There are two isoforms of eIF4G, eIF4GI and eIF4GII, that share 46% sequence identity; in this paper, we refer to both isoforms as "eIF4G" unless indicated otherwise. In addition to recruiting eIF4E and eIF4A, eIF4G interacts with a number of other factors required for efficient translation, including the 40S ribosome-associated eIF3, the poly(A)-binding protein (PABP), and the Ser/Thr kinase Mnk-1 (Prévôt et al., 2003) (Figure 1A). PABP connects eIF4F with the poly(A) tail and thus circularizes the mRNA for increased translational efficiency. Mnk-1 phosphorylates eIF4E, which stimulates translation (Furic et al., 2010).

The middle domain of eIF4G, termed the MIF4G domain, carries out a number of important functions. This segment of approximately 30 kDa mediates protein-protein interactions with eIF4A and eIF3 and also displays RNA and DNA binding capabilities (Ponting, 2000). It has been shown to interact directly with the IRES element of the encephalomyocarditis virus (EMCV) RNA (Pestova et al., 1996; Lomakin et al., 2000) and allows eIF4G to recruit the ribosome to the EMCV RNA in a cap-independent manner by interacting with eIF3 and the RNA at the same time. EMCV is a member of the picornavirus family of viruses, which have the ability to shut down cap-dependent translation initiation in the host. One example of such a mechanism commonly employed by picornaviruses is proteolytic cleavage of eIF4G, resulting in the separation of the eIF4E and PABP binding sites from the rest of the protein and concomitant blockage of cap-dependent translation (Figure 1A). This permits the virus to hijack the translational machinery to efficiently translate its own RNA via IRES-interacting elements in the MIF4G domain.

Cleavage of eIF4G can also occur in noninfected cells during the process of apoptosis, where two caspase cleavage sites in eIF4GI break it into three fragments, thereby impairing cap-dependent translation (Bushell et al., 2000) (Figure 1A). Despite this, it has been observed that the translation of a few specific mRNAs is maintained during apoptosis. The translation of these mRNAs occurs via cap-independent mechanisms that are at least to some extent modulated by the protein

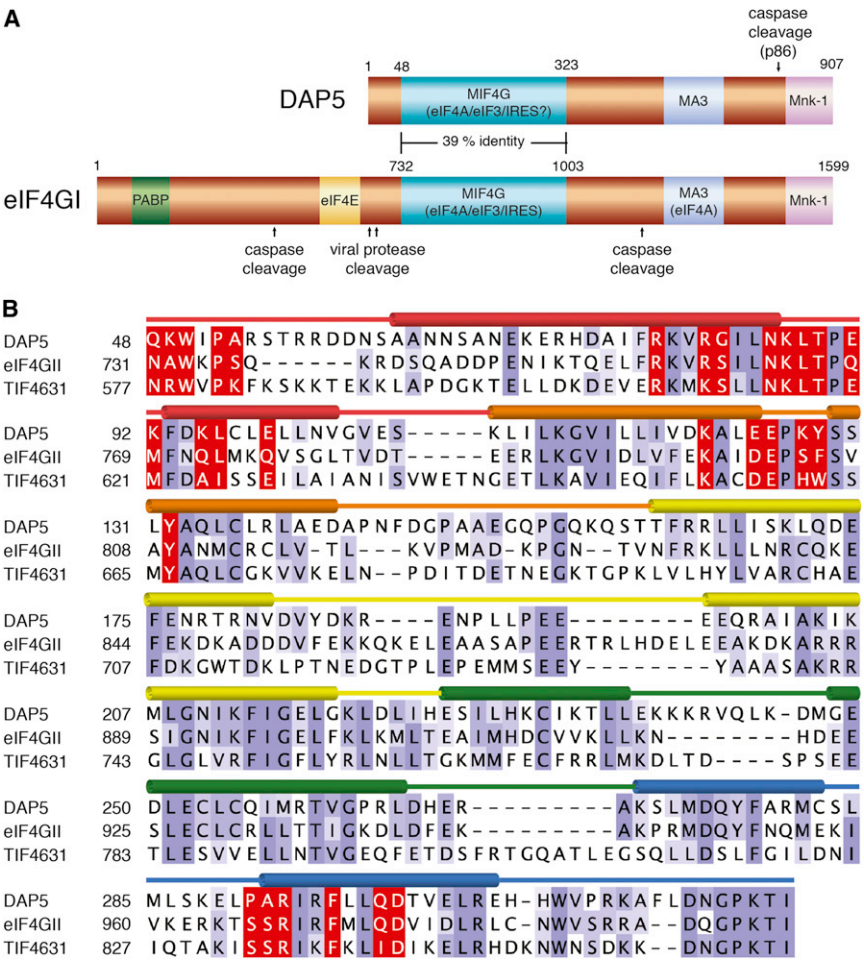

Figure 1. Domain Structure and Sequence Alignment of DAP5 and eIF4G

(A) DAP5 and eIF4GI domain organization highlighting their similarities. Approximate protease cleavage locations are indicated with arrows.

(B) Structure-based sequence alignment of MIF4G domains of human DAP5, human eIF4GII, and TIF4631 (*S. cerevisiae* eIF4G). Residues interacting with eIF4A are highlighted in red. The remainder of the sequence is colored based on conservation using BLOSUM62 scores (Eddy, 2004). Secondary structure elements are shown over the sequence aligned and identified using the same color code as in Figure 2A.

DAP5/p97/NAT1/eIF4G2 (Henis-Korenblit et al., 2000; Lewis et al., 2008; Nevins et al., 2003; Warnakulasuriyarachchi et al., 2004) (DAP5 [Levy-Strumpf et al., 1997]; p97 [Imataka et al., 1997]; NAT1 [Yamanaka et al., 1997]; eIF4G2 [Shaughnessy et al., 1997]). In this paper, we refer to this protein using the "DAP5" nomenclature. DAP5 is homologous to the C-terminal two-thirds of eIF4G and is similar in length to the fragment generated by picornaviral proteolysis (Figure 1A). It is abundantly expressed in proliferating cells (Lee and McCormick, 2006) and contains the important MIF4G domain as well as the MA3 domain. Consistent with its homology to eIF4G, DAP5 interacts with eIF4A and eIF3 but not eIF4E (Imataka et al., 1997; Imataka and Sonenberg, 1997; Yamanaka et al., 1997). However, in contrast to eIF4G, the MA3 domain of DAP5 does not support eIF4A binding (Imataka and Sonenberg, 1997), leaving DAP5 with a single interaction domain for eIF4A as compared to eIF4G's two binding domains.

Because of the lack of an eIF4E binding site, DAP5 is not involved in cap-dependent translation and was reported to be an inhibitor of translation based on overexpression studies (Imataka et al., 1997; Yamanaka et al., 1997). Later it was demonstrated that DAP5 mediates the IRES-driven translation of a number of cellular mRNAs. For example, during apoptosis and other stress conditions, DAP5 specifically enhances the IRES-driven translation of several mRNAs, including those coding for the proteins c-IAP1/HIAP2, XIAP, Apaf-1, c-*myc*, and DAP5 itself (Henis-Korenblit et al., 2000, 2002; Hundsdoerfer et al., 2005; Lewis et al., 2008; Nevins et al., 2003; Warnakulasuriyarachchi et al., 2004).

During apoptosis, DAP5 is cleaved close to the C terminus near its Mnk-1 binding site, generating an 86 kDa fragment that is more active (Figure 1A) (Henis-Korenblit et al., 2000). In addition to its role in apoptosis and stress, DAP5 has also been shown to promote cap-independent translation of cell survival factors during mitosis in unstressed cells (Liberman et al., 2009; Marash et al., 2008). Its reported targets include CDK1 and members of the Bcl family of proteins. The involvement of DAP5 in processes aiding apoptosis, and in cell survival during mitosis, renders it an interesting target for therapy of aberrant cellular states characterized by the dysregulation of apoptosis, such as cancer and autoimmune diseases.

The MIF4G domain of eIF4G and DAP5 is central to their function because it provides a platform for the interaction with eIF4A and eIF3, which are critical for translation initiation. The MIF4G domain of eIF4G was reported to be sufficient to mediate IRES-driven translation initiation (De Gregorio et al., 1998, 1999; Hundsdoerfer et al., 2005; Lomakin et al., 2000), suggesting that the IRES binding determinants of DAP5 may also lie within its MIF4G domain. Surprisingly, however, in spite of their homology and shared functionality, eIF4G and DAP5 can act upon different sets of IRES elements, as in the case of EMCV (Nevins et al., 2003). The MIF4G domain of DAP5 share 39% and 43% sequence identity with eIF4GI and eIF4GII, respectively (Figure 1A). The crystal structure of the MIF4G domain from human eIF4GII revealed a HEAT domain consisting of five pairs of HEAT repeats of antiparallel α helices forming a crescent-shaped right-handed solenoid (Marcotrigiano et al., 2001). Mutational analyses mapped the sites of interaction with eIF4A and potential contacts with IRES RNA to adjacent surfaces on the molecule (Marcotrigiano et al., 2001). There is as yet no structural

information on MIF4G's binding to IRESs. The crystal structure of the yeast eIF4G-eIF4A complex showed that the convex surface of MIF4G makes contact with eIF4A at both its N-terminal and C-terminal regions (Schütz et al., 2008). As in human, yeast also possesses two isoforms of eIF4G. The crystal structure contains isoform I but is referred to as eIF4G throughout the text for simplicity. This structure also revealed a third site of interaction: a conserved tryptophan residue (Trp 579 in yeast eIF4GI also known as TIF4631; Trp 734 in human eIF4GI; Trp 733 in human eIF4GII) at the N terminus of the MIF4G domain anchored to the eIF4A C-terminal domain. Mutation of this residue in yeast eIF4G weakens its interaction with eIF4A and results in the loss of the ability to stimulate eIF4A ATPase activity in vitro and a temperature-sensitive phenotype in vivo (Schütz et al., 2008). This tryptophan residue and most of the residues in the MIF4G domain that make direct contact with eIF4A are conserved in DAP5.

To elucidate the similarities and differences responsible for the crucial functional interactions of the MIF4G domains of DAP5 and eIF4G, we solved the crystal structure of the DAP5 MIF4G domain (hereafter referred to as DAP5M) (Frank et al., 2010). DAP5M adopts the same overall fold as eIF4G but with significant structural differences in some of the helices and their connecting loops that have potential implications for the distinct IRES binding properties of the two proteins. Conserved residues expected to interact with eIF4A are for the most part in the same conformation as seen for the yeast eIF4G-eIF4A complex, and the binding properties of the complex it forms with eIF4AI was investigated by mutational analysis. Additionally, quantitative analysis of the affinity of DAP5M to eIF4A indicates that it is one order of magnitude weaker than that of eIF4GI to eIF4A, which likely underlies DAP5's weaker stimulation of the RNA unwinding activity of eIF4A compared to eIF4GI.

Table 1. Diffraction Data Collection and Refinement Statistics for DAP5M

Data Collection	
X-ray source	CHESS Beamline A1
Wavelength (Å)	0.9785
Resolution (Å)	30–2.3 (2.38–2.3)
Space group	*C2*
Cell parameters (Å, °)	a = 167.630, b = 56.573, c = 74.339, α = 90.00, β = 112.05, γ = 90.00
Molecules per ASU	2
Mosaicity (°)	0.9
Unique reflections	28,017
Redundancy	13.2 (10.5)
I/σ(I)	23.4 (4.8)
Completeness (%)	99.8 (87.5)
R_{sym}	0.107 (0.35)
Refinement	
R_{work}/R_{free}	22.2/25.6
Number of atoms	4,038
Protein	3,837
Ligand/ion	25
Water	176
Rmsd	
Bond lengths (Å)	0.002
Bond angles (°)	0.620
Ramachandran, favored	99.1%
Ramachandran, outliers	0.2%

Rmsd, root-mean-square deviation.

RESULTS

Overall Structure of the DAP5 MIF4G Domain

Based on the crystal structure of the middle domain of eIF4GII, we crystallized and determined the structure of a construct encompassing the middle domain of DAP5 (DAP5M; residues 61 to 323) at 2.3 Å resolution using molecular replacement. Subsequent model building, simulated annealing, energy minimization, and individual B-factor refinement led to final R_{free} and R values of 25.6% and 22.2% (Table 1). DAP5M belongs to the family of HEAT (Huntingtin, Elongation factor 3, PR65/A, and TOR) domains, which are characterized by repeated pairs of antiparallel α helices connected by turns/loops arranged about a common axis (Figure 2A). Each pair of helices (labeled *a* and *b*) constitutes one HEAT repeat, and in DAP5M, ten helices form five HEAT repeats (labeled *1* to *5*), which are stacked on top of each other and stabilized by intervening hydrophobic interactions. Small rotations between the packing of successive HEAT repeats impart a twist to the overall structure, giving rise to a right-handed superhelical axis perpendicular to the repeat helical axes. The MIF4G domain can be subdivided into two smaller subdomains because of the presence of a long 21-residue loop connecting helices 2b and 3a. Thus, subdomain 1 encompasses HEAT repeats 1 and 2 and subdomain 2 includes HEAT repeats 3 to 5. A tilt of ~48° between these subdomains gives the molecule an overall crescent-shaped appearance with two distinctly shaped surfaces, a concave surface and a convex surface (Figure 2A).

The asymmetric unit of the crystal contains two independent copies of DAP5M (chains A and B) related by a 2-fold noncrystallographic symmetry axis (Figure S1 available online). Superposition of the two copies using the Dali server indicates a root-mean-squared deviation (rmsd) of 1.0 Å for 223 corresponding Cα atoms (Holm and Rosenström, 2010). The largest deviations occur at the N terminus, where molecule A is longer by 12 residues in the electron density, and at the C terminus of helix 3a, where the paths of the helices diverge considerably between the two molecules. At approximately residue Val 182, helix 3a of molecule B bends by a few degrees, leading into the connecting loop to helix 3b. In molecule B, this connecting loop is well ordered and modeled in the structure, whereas in molecule A it is completely disordered. Molecule B is better defined in the electron density with regard to the longer loops in the structure, although the average overall backbone B-factors for both molecules are comparable (molecule A: 42.9 $Å^2$; molecule B: 45.2 $Å^2$). The two molecules bury a significant amount of surface area (~2,500 $Å^2$) at their interface; however, the residues in the interface are for the most part polar in nature, and gel filtration analysis of DAP5M indicates a monomeric species in solution (data not shown). Thus, the dimer observed here is likely an artifact of crystallization and probably not physiologically relevant.

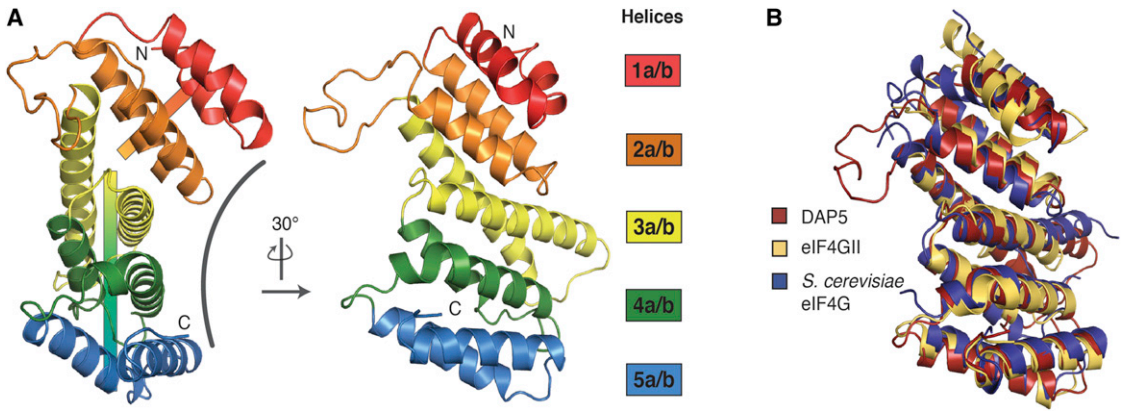

Figure 2. Structural Overview of DAP5M

(A) Ribbon representation of DAP5M. Each HEAT repeat is colored differently. Helix numbering is given on the right. In the left orientation, the concave surface of the protein is indicated with a curved line and colored cylinders within the ribbons denote the superhelical axes. The right orientation, rotated by 30°, highlights the long loop between helices 2b and 3a (colored orange), which causes the molecule to be divided into two subdomains. See Figure S1.

(B) Structural superposition of DAP5M with the MIF4G domains of human eIF4GII (PDB ID code 1HU3) and *S. cerevisiae* eIF4G (TIF4631; PDB ID code 2VSO). All molecular figures were generated using the program PyMol (The PyMOL Molecular Graphics System, v.1.2r3pre, Schrödinger).

Comparison of DAP5M and eIF4G MIF4G Domains

Two crystal structures of the MIF4G domain from eIF4G have been determined previously: that from human eIF4GII and the structure of the *Saccharomyces cerevisiae* eIF4G middle domain in complex with eIF4A (Marcotrigiano et al., 2001; Schütz et al., 2008). Human DAP5 shares 43% and 32% sequence identity (based on structure-based sequence alignments) with human eIF4GII and *S. cerevisiae* eIF4G, respectively, in their MIF4G domains and all of them adopt the same overall fold (Figure 2B). Superposition of DAP5M on human and yeast eIF4G using the Dali server indicates rmsd values of 1.7 Å and 2.6 Å, based on 190 and 212 corresponding Cα atoms, respectively (Holm and Rosenström, 2010). However, there are significant differences observed in the length and orientation of a number of helices. Additionally, the loops connecting the helices differ considerably in length and conformation. In particular, the concave side of the molecule in the N-terminal region opposite the eIF4A binding site encompassing the helices of HEAT repeats 1, 2, and 3 and the loop connecting repeats 2 and 3 display very different conformations (Figure 2B). The loop connecting repeats 2 and 3 (residues 142 to 161) is 18 residues in length and extends outward from the otherwise very compact structure of the HEAT domain. In the eIF4GII structure, this loop is largely disordered and shorter by six residues. Other notable differences occur in the loop connecting helices 3a and 3b (residues 185 to 200), which is well ordered in DAP5 and disordered in eIF4GII, where it is longer by 12 residues, and the loop connecting helices 4a and 4b (residues 236 to 249), which is longer in DAP5 by 7 residues. Large structural differences such as these impart significant differences in shape and chemical attributes to their surfaces and likely contribute to the functional differences observed between these proteins, such as IRES binding.

Identification of a Potential IRES Binding Site in DAP5M

Although eIF4G and DAP5 have common protein binding partners in eIF4A and eIF3, their interactions with nucleic acids are distinct. In vitro studies of human eIF4GI have demonstrated that its MIF4G domain is able to interact with different RNAs, namely, the EMCV IRES RNA and β-globin mRNA (Pestova et al., 1996; Lomakin et al., 2000), and one study even reported interaction with DNA (Kim et al., 1999). The DAP5 MIF4G domain, on the other hand, does not interact with the EMCV IRES RNA or β-globin mRNA in vitro (Lomakin et al., 2000). Several studies have suggested that DAP5 can initiate translation via IRES elements found in a number of cellular mRNAs (Henis-Korenblit et al., 2000, 2002; Hundsdoerfer et al., 2005; Lewis et al., 2008; Nevins et al., 2003; Warnakulasuriyarachchi et al., 2004). This raises the question as to whether DAP5M interacts with these IRES elements in a manner similar to how eIF4G associates with the EMCV IRES for cap-independent translational initiation.

To identify potential sites of IRES interaction, we show the solvent-accessible surface of DAP5M colored according to its electrostatic potential in Figure 3A. In the N-terminal region of the molecule, there exists a large area of positively charged surface, which could potentially interact with nucleic acid. Interestingly, we found a sulfate ion from the crystallization buffer bound to a cluster of positively charged residues (Lys 108, Lys 112, and Arg 165) in this region (Figure 3A). This interaction could potentially mimic electrostatic interactions of the phosphodiester backbone of IRES RNA with DAP5M. The positively charged area corresponds to a highly conserved region among various orthologs of DAP5 (Figures 3B and S2). Comparison of the equivalent surface in human eIF4GII also reveals large patches of positive potential but with significantly different distribution of the charges, perhaps owing to the distinct IRES targeted by these two proteins (Figure 3C).

The positively charged region in DAP5M is adjacent to the eIF4A-binding site (see below), suggesting that IRES binding may be coupled to the interaction with eIF4A. In support of this, a previous analysis of the MIF4G domain from eIF4GII identified mutants that affect binding of both eIF4A and the EMCV IRES (Marcotrigiano et al., 2001). Furthermore, the IRES interaction is enhanced in the presence of eIF4A (Lomakin et al., 2000).

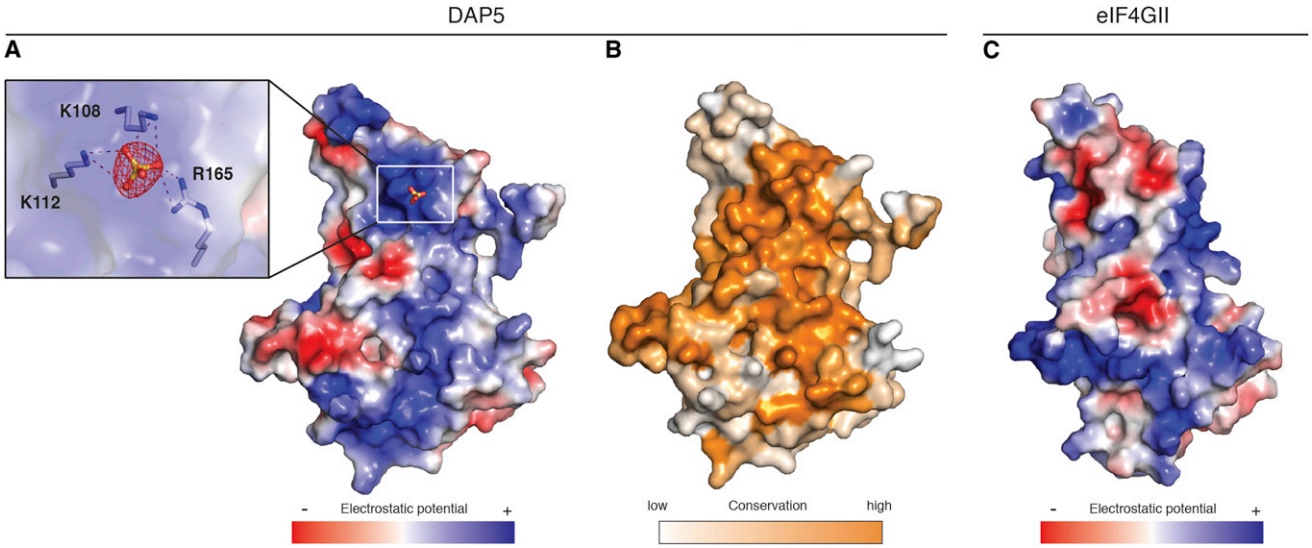

Figure 3. Surface Properties of DAP5M and MIF4G Domain from eIF4GII

(A) Electrostatic potential surface representation of DAP5M. The surface was calculated using APBS (Baker et al., 2001): red $<-3k_BT/e$ and blue $>+3k_BT/e$, where k_B denotes Boltzmann constant and T denotes temperature. Inset: Enlargement of electrostatic surface surrounding the observed sulfate ion found on molecule B of DAP5M.

(B) Mapping of the surface conservation using selected eukaryotic DAP5 orthologs (see Figure S2).

(C) Electrostatic potential surface representation of the MIF4G domain from eIF4GII (PDB ID code 1HU3).

These observations indicate that there is cooperativity in binding of eIF4A and RNA to eIF4G and that the sites of interaction are probably in close proximity to one another. Considering the functional and structural homology between eIF4G and DAP5, it is likely that DAP5M utilizes a similar mode of cooperative binding to eIF4A and IRES RNA. Based on our crystal structure of DAP5M, it will be possible to carry out a mutational analysis of the residues in this region to confirm its role in DAP5-mediated IRES-driven translation initiation.

The Sites of Interaction with eIF4A Are Structurally Conserved in the Middle Domains of eIF4G and DAP5 but Have Different Binding Affinities

It was previously shown that DAP5M, like eIF4G, recruits eIF4A, a member of the DEAD box RNA helicase family (Imataka et al., 1997). eIF4A is a 46 kDa bilobal protein with its N- and C-terminal domains connected by a flexible linker. Given the conservation of the overall folds of the MIF4G domains of DAP5 and eIF4G, it is likely that they interact with eIF4A in the same manner. To analyze the potential site of eIF4A interaction on DAP5M, we constructed a model of the complex by superposition of the DAP5M structure onto the crystal structure of the *S. cerevisiae* eIF4G-eIF4A complex (Schütz et al., 2008) (Figure 4). As with the yeast eIF4G-eIF4A complex, the DAP5M-eIF4A model reveals that there are two main sites of interaction between the two proteins. The C-terminal domain of eIF4A interacts with the N-terminal region of DAP5M encompassing heat repeats 1 and 2 (Site 1), whereas the N-terminal domain of eIF4A makes contact with the C-terminal part of DAP5M on helix 5b (Site 2). Together, the two sites of interaction bury ~2,100 $Å^2$ of surface area at the interface. Additionally, a third site of interaction in the yeast eIF4G-eIF4A complex was identified, which is contributed by a tryptophan residue connected to the MIF4G domain through a flexible, N-terminal linker that buries it in the C-terminal domain of eIF4A (Schütz et al., 2008). This conserved tryptophan residue, although present in DAP5 (Trp 50), could not be modeled as it was not included in our crystallization construct due to its likely flexible attachment. However, the contribution of Trp 50 to the interaction of DAP5 with eIF4A in humans is marginal, as observed in our binding and activity assays in vitro (data not shown). This suggests that, unlike what is observed in yeast, Trp 50 may not be as essential for DAP5's interaction with eIF4A or its effect may be more subtle in humans and will require other assays to fully characterize its role.

Yeast eIF4GI middle domain and DAP5M have only 32% identity, yet the majority of eIF4A-interacting residues in eIF4G (19 of 24 total interface residues), as identified in the crystal structure of the complex, are conserved in DAP5 (Figure 1B). Importantly, the model of the DAP5M-eIF4A complex indicates that, in addition to the sequence, the conformations of most of the residues at the interface are also conserved, even in the absence of eIF4A. Of the 24 residues that make contact at Site 1 and Site 2, approximately three-quarters are in very similar conformations (Figure 4). This suggests that the binding mode between DAP5 and eIF4A mirrors that of eIF4G and that the interaction occurs through, for the most part, a preformed binding site on DAP5. Thus, we expected the binding affinities of eIF4A for the MIF4G domains of eIF4G and DAP5 to be comparable.

To ascertain whether this is indeed the case, we carried out isothermal titration calorimetry (ITC) experiments to compare dissociation constants for the interaction of human eIF4A (isoform I) with the MIF4G domains of human eIF4G (isoform I: 81% identical to eIF4GII in their MIF4G domains) and DAP5. Both constructs included the conserved tryptophan residue (Trp 50 in DAP5; Trp 734 in eIF4GI) as described in yeast. We measured a dissociation constant of 0.136 μM for the binding

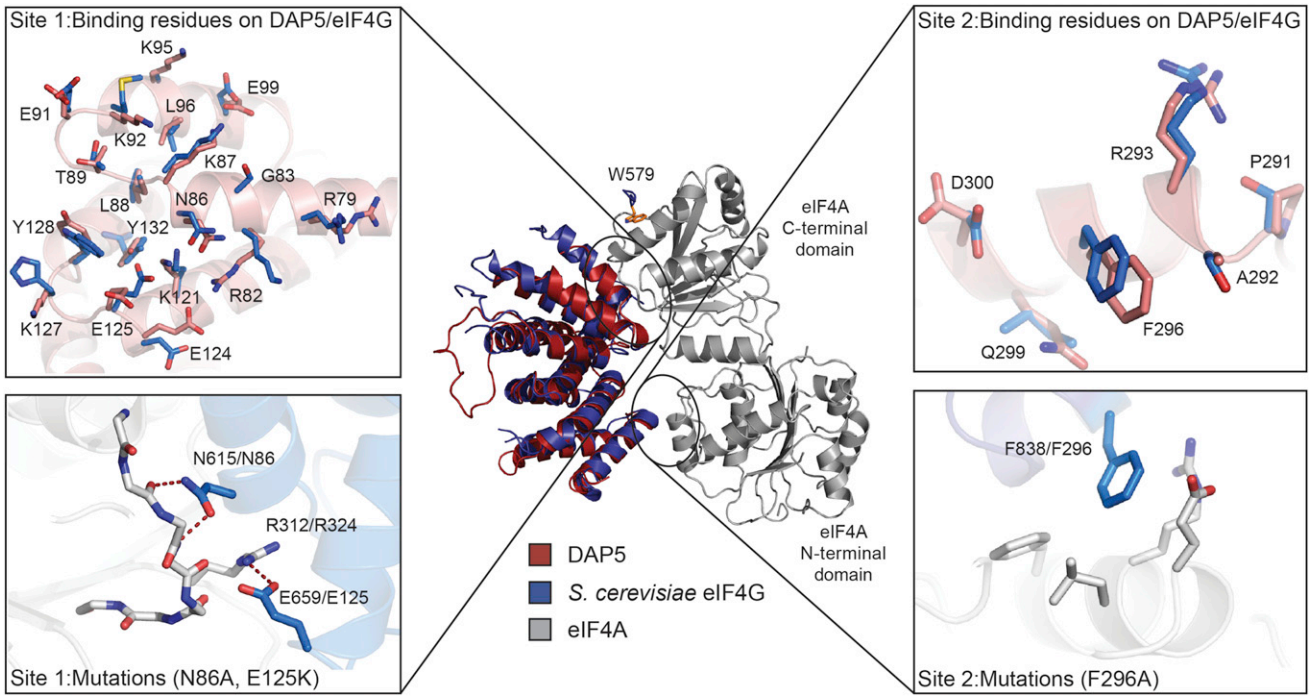

Figure 4. Model of the DAP5M-eIF4A Complex

Center: Shown is the crystal structure of the yeast eIF4G-eIF4A complex (purple-gray) with DAP5M (red) superimposed on eIF4G. W579 (W50 in DAP5M), which comprises the third interaction site in the eIF4G-eIF4A complex, is represented as orange sticks. Left: Detailed view of Site 1 interaction residues. Top: Residues on the surface of eIF4G and DAPM that interact with eIF4A are shown as sticks. The view is rotated relative to the orientation in the center panel. Nitrogen, oxygen, sulfur, and carbon atoms are colored blue, red, yellow, and pink (DAP5M)/light blue (eIF4G), respectively. The majority of residues are conserved in sequence and conformation. Labels for residue numbers are shown for DAP5M only. Bottom: Selected residues from the yeast eIF4G structure (light-blue carbon atoms) that interact with yeast eIF4A (white carbon atoms) for which the corresponding residues in DAP5M were mutated. Labels for residue numbers from both yeast eIF4G/eIF4A and human DAP5/eIF4AI are indicated. Right: Detailed view of Site 2 interaction residues with similar coloring and labeling scheme as above.

of eIF4A to eIF4G with a stoichiometry of 1:1 (Figure 5A). This is in agreement with the crystal structure of the yeast eIF4G-eIF4A complex and our gel filtration analysis (Figure S3), which both show one molecule of eIF4A bound to a single MIF4G domain. Surprisingly, we found that the affinity of DAP5M for eIF4A is only 1.1 μM—about 10-fold lower than that of eIF4G, also with a stoichiometry of 1:1 (Figure 5B). This suggests that despite the conservation of the binding site in both sequence and structure, other residues outside of the binding site modulate the affinity of MIF4G domains for eIF4A binding. Alternatively, it may be possible that the few nonconserved residues in the interface reduce the binding affinity or that the model of DAP5M-eIF4A based on the yeast complex does not accurately reflect the actual mode of binding altogether.

Mutational Analysis of Site 1 and Site 2 Residues in the DAP5-eIF4A Complex

To examine whether residues predicted by the model of the DAP5M-eIF4A complex are indeed important in the interaction, we mutated conserved residues in DAP5M at the Site 1 and Site 2 interfaces and carried out in vitro binding studies. At Site 1 we chose to mutate two key interactions: Asn 86 to alanine (N86A) and Glu 125 to lysine (E125K). Asn 86 forms several hydrogen bonds with backbone atoms from a loop in the C-terminal lobe of eIF4A and Glu 125 makes a salt bridge with Arg 312 of yeast eIF4A (Arg 324 in human eIFAI), also located on a loop in the C-terminal lobe (Figure 4, lower left panel). At Site 2, Phe 296, which makes interactions with a hydrophobic pocket on the N-terminal lobe of eIF4A, was mutated to alanine (F296A) (Figure 4, lower right panel). These mutant proteins were soluble as exhibited by their well-behaved gel filtration profiles (Figure S3). Mutation of single residues at either the Site 1 or Site 2 interfaces resulted in complete loss of binding in in vitro pull-down assays (Figure 6A). The same results were obtained using gel filtration chromatography (Figure S3). Our results agree with those obtained by Morino et al. (2000), who showed that the mutation of Phe 977 (equivalent to Phe 296 in DAP5) to Ala (F977A) in eIF4GI resulted in loss of binding to eIF4A in cell extracts. This confirms that DAP5M interacts with eIF4A in the same manner as was observed for eIF4G, albeit with a lower affinity, which may impact its ability to stimulate eIF4A activity.

Effect of DAP5M on the Helicase Activity

To assess the effect of the lower affinity DAP5M-eIF4A interaction on helicase activity, we used a fluorescence-based activity assay to monitor RNA unwinding by full-length human eIF4A in vitro (Özeş et al., 2011). The stimulation of eIF4A helicase activity through interaction with eIF4G is well established in vitro using either protein purified from cell extracts or recombinant protein, although the extent of stimulation depends on the particular construct used (Abramson et al., 1988; Rogers et al., 2001). Full-length eIF4G, however, is intrinsically unstable, and

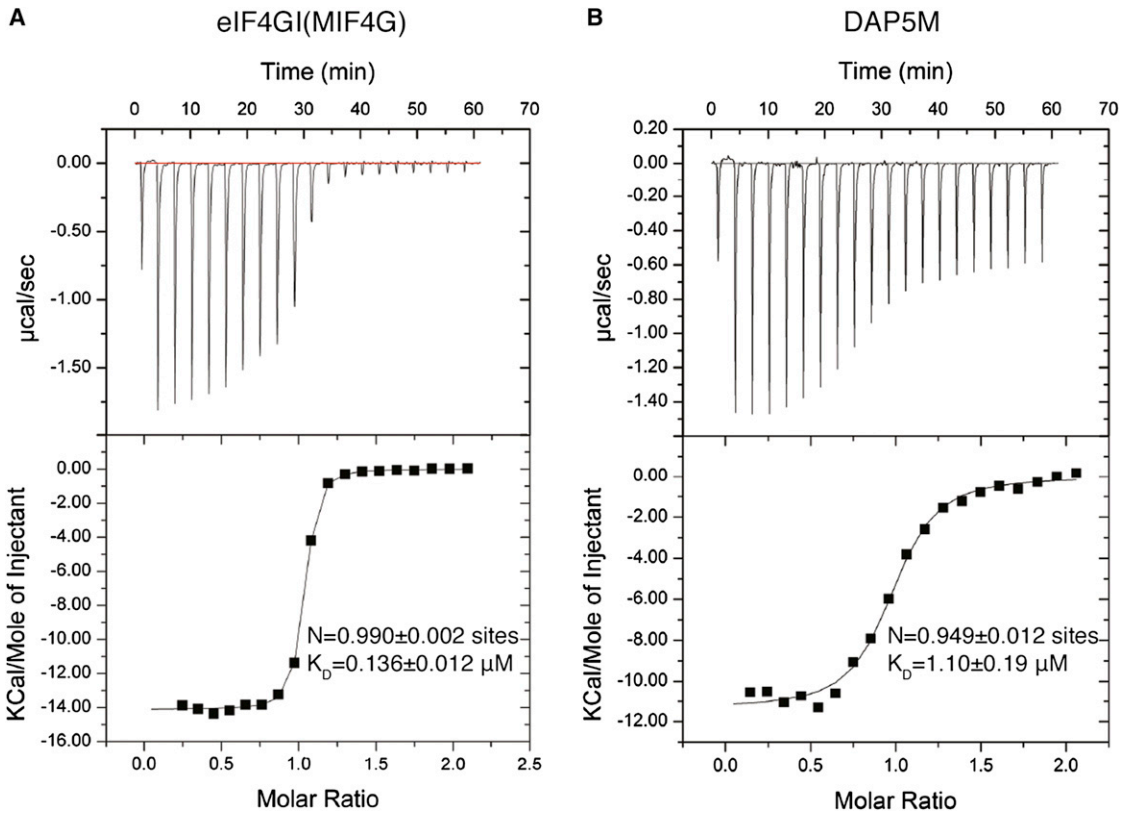

Figure 5. ITC Titration Binding Curves

(A) eIF4AI with eIF4GI(MIF4G) (residues 732–1003), where K_D is the dissociation constant and N is the number of binding sites.

(B) eIF4AI with DAP5M (residues 48–323).

thus, for our activity assays, we used a construct encompassing approximately the C-terminal two-thirds of eIF4G, lacking regions upstream of the MIF4G domain (residues 732–1571), similar to one previously demonstrated to robustly stimulate eIF4A ATPase activity in vitro (Korneeva et al., 2005). Analogously for DAP5, we used a near full-length construct beginning just N-terminal to the middle domain and extending to the C terminus (residues 48–907). The reaction mix also includes the accessory factor eIF4B, which enhances eIF4A processivity (Rogers et al., 2001).

eIF4A and eIF4B display relatively low unwinding activity on their own (Figure 7, green). Addition of wild-type DAP5$^{48–907}$ to the reaction almost doubled the basal unwinding rate to 4.5% per minute (Figure 7, red). The N86A mutant of DAP5$^{48–907}$, which as demonstrated above abrogates binding of eIF4A to DAP5M, returned the activity back to basal levels (Figure 7, lavender), confirming the importance of DAP5-eIF4A binding for stimulation of RNA unwinding activity. Thus, as with eIF4G, DAP5 can stimulate eIF4A activity via interaction with its middle domain. However, carrying out the unwinding reaction with eIF4G$^{732–1571}$ in our assay indicates that it is twice as potent as DAP5$^{48–907}$ in stimulating helicase activity (Figure 7, blue). For the above-mentioned experiments, all of the proteins in the reaction mixtures were maintained at concentrations of 1 µM. According to the dissociation constants determined above for the middle domains, at 1 µM concentration DAP5$^{48–907}$ would be less occupied by eIF4A than eIF4G$^{732–1571}$, which would be close to saturation, although the precise situation is more complex because eIF4G$^{732–1571}$ contains a second binding site for eIF4A in its C-terminal region that is absent in DAP5$^{48–907}$. Nonetheless, the 10-fold difference in binding affinity of eIF4A with the middle domains of the two proteins likely contributes to the observed differences in their respective stimulation of unwinding activities. Indeed, increasing the DAP5$^{48–907}$ and eIF4G$^{732–1571}$ concentrations to 2 µM in the assay (Figure 7, gray and gold) substantially reduces the observed difference in unwinding activities between the two proteins.

DISCUSSION

We have determined the crystal structure of the MIF4G domain from DAP5. Our structure reveals that the overall fold of DAP5M is a helical HEAT domain that is very similar to that found in crystal structures of the MIF4G domain from eIF4G. However, significant conformational differences in the connecting loop structures of DAP5M impart distinct shape and surface characteristics to it. We also showed that DAP5M is functionally homologous to eIF4G in its ability to interact with and stimulate eIF4A activity.

A precise molecular role for DAP5 is still lacking. The earliest reports, via overexpression in vitro and in transfected cells, ascribed an inhibitory role to DAP5 on both cap-dependent

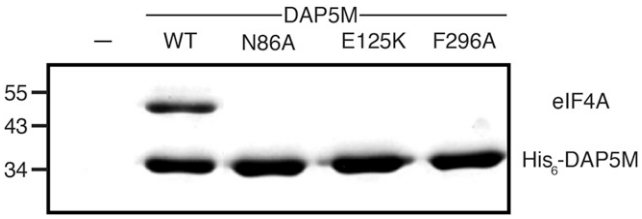

Figure 6. In Vitro Pull-Down Experiments
Hexahistidine-tagged constructs of purified DAP5M and its mutants were used as bait and purified eIF4AI as prey. Shown are Coomassie Brilliant Blue-stained SDS-PAGE gels. Indicated on the left are protein marker sizes in kDa. Pull-downs of eIF4A with DAP5M contain mutations at Site 1 or Site 2. Lane 1 is a control in which eIF4A alone is incubated with empty Ni-NTA beads to account for nonspecific binding of eIF4A to the resin. Lane 2 is a positive control with wild-type DAP5M, which shows strong binding to eIF4A. Lanes 3 to 5 are pull-downs with the indicated mutants of DAP5M, all three of which fail to pull down eIF4A. See Figure S3.

and EMCV-IRES-driven translation. Based on this, it was postulated that DAP5 could function as a general translation inhibitor by sequestering eIF4A and eIF3, but not eIF4E, into inactive complexes. Later studies often produced many conflicting results with functions of DAP5 ranging from inhibitor of cap-dependent translation (Henis-Korenblit et al., 2002), stimulator of DAP5 IRES-dependent translation (Nevins et al., 2003), inert in DAP5 IRES-dependent translation (Henis-Korenblit et al., 2002), and even a stimulator of cap-dependent translation (Lee and McCormick, 2006). All of these studies were based on overexpression of DAP5 beyond physiological levels, which could account for the varying results observed, depending on the precise conditions and cell types used.

Much evidence now points to DAP5 being a scaffolding protein in IRES-mediated translation. Knockout and knockdown studies have established that DAP5 is an essential factor for the translation of specific cellular mRNAs containing IRES elements in their 5′-UTRs, such as c-*myc*, CDK1 and Bcl family members, and DAP5 itself (Yamanaka et al., 2000; Marash et al., 2008). However, the molecular details of how DAP5 partakes in translation initiation and its relationship to eIF4G have remained elusive. Our structure of DAP5M supports its role in IRES-mediated translation in that it possesses a positive surface charge distribution distinct from that found in MIF4G and is well-suited for interaction with nucleic acids, although direct interaction between DAP5M and IRES RNA remains to be demonstrated.

Our finding of a 10-fold affinity difference between eIF4A and the middle domains of eIF4G and DAP5 resulting in variable stimulation eIF4A helicase activity further supports the notion that DAP5 does not simply function as a general translational inhibitor. eI4FA is the most abundant initiation factor present in the cell, present at concentrations of up to ~30 μM, whereas DAP5/eIF4G levels can be in the range of ~2 to 6 μM (Duncan and Hershey, 1983; Lee and McCormick, 2006). Thus, based on the dissociation constants determined here, both DAP5 and eIF4G would for the most part be in complex with eIF4A, although DAP5 is likely more dynamic in this regard, owing to its lower affinity for eIF4A. Indeed, the levels of DAP5 are significantly modulated under cellular stress conditions, particularly during caspase activation, which causes a shift from cap-dependent to cap-independent translation by the degradation of eIF4G (Bushell et al., 2000; Svitkin et al., 1999; Henis-Korenblit et al., 2000), thereby favoring the association of DAP5 with eIF4A.

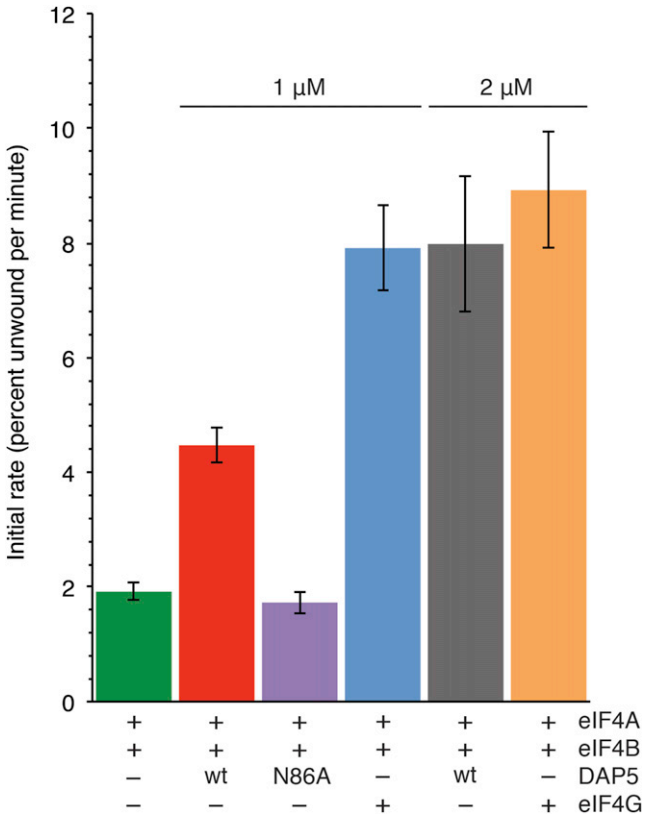

Figure 7. In Vitro Helicase Assay
The percent unwinding of the RNA substrate over time was monitored by measuring the increase in fluorescence caused by eIF4A and eIF4B in the absence (green) or in the presence of wild-type DAP5 (red and gray) or its N86A mutant (lavender), or in presence of the C-terminal two-thirds of eIF4G (blue and gold). Each protein was present at 1 μM in the unwinding reaction unless specified otherwise. The initial unwinding rates were extracted from the initial linear portion of the unwinding time course and expressed as percent unwinding per minute. Error bars represent the standard deviation of three replicates. Wild-type DAP5 and its eIF4G equivalent stimulate the activity of the helicase, whereas unwinding in the reaction containing DAP5 N86A is comparable to that of eIF4A and eIF4B alone. There is an ~2-fold difference in unwinding aided by DAP5 and eIF4G at 1 μM, but their eIF4A-stimulation capacities are more similar at 2 μM.

Finally, the importance of the DAP5-eIF4A interaction was further validated in recent translation rescue experiments from rabbit reticulocyte lysate, where the ability of recombinant DAP5 to rescue the translation of cellular IRESs depended specifically on the integrity of interaction between its middle domain and eIF4A (V. Gandin, personal communication). Future studies aimed at deciphering the molecular contribution of DAP5 to IRES-driven translation will be required to unravel its true biological role.

EXPERIMENTAL PROCEDURES

Expression and Purification of Recombinant Proteins

The MIF4G domain of human DAP5 (DAP5M; residues 48 to 323 and 61 to 323) was subcloned into the BamHI and EcoRI restriction sites of the bacterial

expression vector pProEx HTb (Invitrogen, Carlsbad, CA, USA). DAP5M was expressed in *Escherichia coli* strain BL21 (Rosetta 2) by induction at OD_{600} = 0.6 with 1 mM isopropyl-β-D-thiogalactoside (IPTG) for 4 hr at 30°C. The protein was purified by nickel affinity chromatography on a Sepharose 6 Fast Flow nickel affinity resin column (HisTrap FF, GE Healthcare, Little Chalfont, UK). Following overnight TEV cleavage and dialysis against nickel binding buffer, TEV protease (hexahistidine-tagged) was removed by applying samples onto a HisTrap FF column and collecting the flowthrough. Tagged and cleaved protein was further purified by gel filtration chromatography on a HiLoad 16/60 Superdex 75 prep grade column (GE Healthcare) eluted with a buffer containing 25 mM Tris (pH 8.0), 150 mM NaCl, 5% glycerol, 1 mM phenylmethylsulfonyl fluoride (PMSF), and 1 mM dithiothreitol (DTT).

Human full-length eIF4AI was cloned into the BamHI and EcoRI restriction sites of the bacterial expression vector pProEx Htb (Invitrogen). The protein was expressed in *E. coli* strain BL21 (DE3) by autoinduction at OD_{600} = 0.6 overnight at 20°C (Studier, 2005). The protein was purified by nickel affinity chromatography and cleaved as described for DAP5M. The cleaved protein was further purified by anion exchange chromatography on a Q Sepharose Fast Flow resin column (HiTrap Q FF, GE Healthcare) before gel filtration, as described for DAP5M.

The middle domain of human eIF4GI (MIF4G, residues 732 to 1003) was cloned into pET-28b-SMT3 vector (Mossessova and Lima, 2000), in which we mutated the EcoRI restriction site originally contained in the SUMO coding region, enabling the use of EcoRI as forward restriction site together with XhoI. A longer eIF4G construct encompassing its three HEAT-repeats domains (732–1571) was cloned into the BamHI and NotI sites of the same vector. The purification steps for MIF4G and $eIF4G^{732\text{-}1571}$ are the same as for DAP5M and eIF4A, respectively. Ulp-1 was used to desumoylate the fusion proteins (Mossessova and Lima, 2000).

Human DAP5 (residues 48 to 907) was cloned into pProEx Htb (Invitrogen) and expressed as an N-terminal hexahistidine fusion protein in *E. coli* strain BL21 (Rosetta 2) by autoinduction overnight at 20°C (Studier, 2005). The protein was purified by nickel affinity chromatography on Ni-NTA Superflow resin (QIAGEN, Hilden, Germany) followed by anion exchange chromatography on a Q Sepharose Fast Flow resin column (HiTrap Q FF, GE Healthcare). The protein was further purified by gel filtration chromatography on a Superdex 200 HR 10/300 column (GE Healthcare) eluted with a buffer containing 25 mM Tris (pH 8.0), 150 mM NaCl, 5% glycerol, 1 mM phenylmethylsulfonyl fluoride (PMSF), and 3 mM dithiothreitol (DTT).

All DNA sequences were confirmed by sequencing.

Mutagenesis of DAP5M

Mutants of DAP5M (48–323) and DAP5 were generated using the QuikChange mutagenesis kit (Stratagene, La Jolla, CA, USA). Sequences of the mutants were confirmed by plasmid DNA sequencing. The mutant proteins were expressed and purified as described above for the wild-type protein.

Crystallization and Data Collection

Tris(2-carboxyethyl)phosphine (TCEP; 1 mM final concentration) was added to DAP5M (61–323) samples before use in crystallization trials. Crystals suitable for structure determination were grown at 291 K using protein concentration of 15–20 mg/ml in drops of 2–4 μl volume (1–2 μl protein solution mixed with 1–2 μl reservoir solution). Crystals were grown in 0.1 M HEPES (pH 7.5), 0.2 M ammonium sulfate, and 18%–20% (w/v) polyethylene glycol 5000 monomethyl ether (PEG 5000 MME). Crystals were flash-cooled in a liquid-nitrogen cryostream at 100 K, and data were collected in-house on a Rigaku MicroMax-007 HF microfocus X-ray generator fitted with Varimax X-ray optics and a Saturn 944+ CCD detector.

Structure Determination

Crystallization, data collection, and initial structure solution of DAP5M were carried out as described previously (Frank et al., 2010). In short, DAP5M shares ~43% sequence identity with its homologous region in eIF4GII. Crystals belong to the space group *C*2 with two molecules of DAP5M per asymmetric unit and diffracted to 2.4 Å (Table 1). Maximum likelihood molecular replacement using the program *Phaser* (Read, 2001) and the structure of the eIF4GII MIF4G domain (Protein Data Bank [PDB] ID code 1HU3; Marcotrigiano et al., 2001) resulted in a solution with acceptable Z scores and log-likelihood gain (RFZ = 5.3; TFZ = 11.3; LLG = 169). However, initial attempts at refinement did not reduce the R factors. Therefore, we broke up the *Phaser* solution into 20 separate rigid bodies, each corresponding to one helix and carried out rigid body refinement. This reduced the R factors to 47%, and subsequent simulated annealing, energy minimization, and B-factor refinement with the program CNS (Brünger et al., 1998), as well as density modification, including the application of 2-fold NCS symmetry averaging using the program *DM* (Cowtan and Main, 1993), further reduced the R factors and resulted in reasonable electron density for majority of the structure allowing us to build a model. During initial refinement against the home source data set described before (Frank et al., 2010), *CNS* (Brünger et al., 1998) was used and NCS restraints were applied. This refinement resulted in a final model with an R_{free} and R factor of 27.8% and 24.4%, respectively. The resulting model was then further refined against a slightly higher resolution data set (2.3 Å) from CHESS beamline A1 (Table 1) using *Phenix* (Adams et al., 2002). NCS restraints were removed for refinement using *Phenix*, but TLS refinement was employed. The final model yielded an R factor of 22.2% and R_{free} of 25.6%.

Gel Filtration Chromatography

Half milliliter samples containing 0.5 mg His-DAP5M (or MIF4G, or eIF4A alone) with or without 0.5 mg eIF4A were injected over a Superdex 200 10/300 GL column (GE Healthcare) eluted with a buffer containing 25 mM Tris (pH 8.0), 150 mM NaCl, and 5% glycerol.

In Vitro Pull-Down Assays

Thirty micrograms of His-DAP5M were incubated in binding buffer (25 mM Tris [pH 8.0], 150 mM NaCl, 60 mM imidazole [pH 8.0], and 5% glycerol) together with 25 μl Ni-NTA Superflow resin (QIAGEN) and 100 μg of eIF4AI (~3-fold molar excess) for 30 min on ice in 100 μl reaction volume. After washing with 3 × 700 μl of binding buffer, proteins were eluted with 50 μl of elution buffer (25 mM Tris [pH 8.0], 500 mM NaCl, and 500 mM imidazole [pH 8.0]). SDS-PAGE was carried out on a 12% polyacrylamide gel and eluted proteins were visualized with Coomassie Brilliant Blue staining.

Isothermal Titration Calorimetry

Experiments were performed with a VP-ITC instrument (MicroCal, GE Healthcare) at 20°C. His-DAP5M (or desumoylated MIF4G from eIF4GI) and eIF4AI samples were first dialyzed against a buffer containing 25 mM Tris (pH 8.0), 150 mM NaCl, and 1 mM DTT and then diluted to 0.5–1.0 mM and 0.05–0.1 mM, respectively. MIF4G domain proteins were loaded into the syringe, whereas eIF4AI was loaded into the calorimetric cell. The heat of binding was measured over the injection of 37 μl of MIF4G in 2 μl increments into the cell. Data were fitted to a one binding site model using the Origin software package (MicroCal, GE Healthcare).

Helicase Assays

Experiments were performed as described by Özeş et al. (2011). eIF4A, eIF4B, DAP5, and eIF4G were used at a concentration of 1 μM unless specified otherwise. The substrate is a double-reporter RNA construct with a 20 nt 5′ overhang and a 24 bp duplex region. It was used at a concentration of 50 nM. Sequences are as follows, with underlined regions corresponding to the duplex regions: template: 5′-GAACAACAACAACAACAACAGAAAAAAUUAAAAAAAUUAAAAAACUCGGAGGGGCCGGUGGGGCC – 3′; Cy3 strand sequence: 5′-Cy3- GUUUUUUAAUUUUUUAAUUUUUUC – 3′; BHQ strand sequence: 5′- GGCCCCACCGGCCCCUCCG – BHQ – 3′; 24-nt DNA competitor: 5′- GAAAAAATTAAAAAATTAAAAAAC – 3′.

BHQ and Cy3-labeled RNA oligonucleotides were annealed side-by-side (one nucleotide apart) to the template RNA. Competitor DNA was present in 10x excess to capture Cy3 RNA upon unwinding.

ACCESSION NUMBERS

The atomic coordinates for the MIF4G domain of DAP5 have been deposited in the Protein Data Bank under ID code 4IUL.

SUPPLEMENTAL INFORMATION

Supplemental Information includes three figures and can be found with this article online at http://dx.doi.org/10.1016/j.str.2013.01.015.

ACKNOWLEDGMENTS

We thank R. Szittner and K. Illes for technical support. B.N. is supported by a Canada Research Chair, a Career Development Award from the Human Frontiers Science Program (CDA 0018/2006-C/1), and an operating grant from the Canadian Institutes of Health Research (CIHR grant MOP-82929). N.S. is funded by a CIHR grant. C.F. and K.F. are supported by grant R01GM092927 from the National Institute of General Medical Sciences and a National Institutes of Health training grant (T32 GM-007377-29 to K.F.). G.V. is supported by the CIHR Strategic Training Initiative in Chemical Biology and by the Groupe de Recherche Axé sur la Structure des Protéines (FRSQ). M.S. was supported by an NSERC-CREATE Training Program in Bionanomachines Undergraduate Award.

Received: January 27, 2012
Revised: December 24, 2012
Accepted: January 19, 2013
Published: March 7, 2013

REFERENCES

Abramson, R.D., Dever, T.E., and Merrick, W.C. (1988). Biochemical evidence supporting a mechanism for cap-independent and internal initiation of eukaryotic mRNA. J. Biol. Chem. *263*, 6016–6019.

Adams, P.D., Grosse-Kunstleve, R.W., Hung, L.W., Ioerger, T.R., McCoy, A.J., Moriarty, N.W., Read, R.J., Sacchettini, J.C., Sauter, N.K., and Terwilliger, T.C. (2002). PHENIX: building new software for automated crystallographic structure determination. Acta Crystallogr. D Biol. Crystallogr. *58*, 1948–1954.

Baker, N.A., Sept, D., Joseph, S., Holst, M.J., and McCammon, J.A. (2001). Electrostatics of nanosystems: application to microtubules and the ribosome. Proc. Natl. Acad. Sci. USA *98*, 10037–10041.

Brünger, A.T., Adams, P.D., Clore, G.M., DeLano, W.L., Gros, P., Grosse-Kunstleve, R.W., Jiang, J.S., Kuszewski, J., Nilges, M., Pannu, N.S., et al. (1998). Crystallography & NMR system: A new software suite for macromolecular structure determination. Acta Crystallogr. D Biol. Crystallogr. *54*, 905–921.

Bushell, M., Poncet, D., Marissen, W.E., Flotow, H., Lloyd, R.E., Clemens, M.J., and Morley, S.J. (2000). Cleavage of polypeptide chain initiation factor eIF4GI during apoptosis in lymphoma cells: characterisation of an internal fragment generated by caspase-3-mediated cleavage. Cell Death Differ. *7*, 628–636.

Cowtan, K.D., and Main, P. (1993). Improvement of macromolecular electron-density maps by the simultaneous application of real and reciprocal space constraints. Acta Crystallogr. D Biol. Crystallogr. *49*, 148–157.

De Gregorio, E., Preiss, T., and Hentze, M.W. (1998). Translational activation of uncapped mRNAs by the central part of human eIF4G is 5′ end-dependent. RNA *4*, 828–836.

De Gregorio, E., Preiss, T., and Hentze, M.W. (1999). Translation driven by an eIF4G core domain in vivo. EMBO J. *18*, 4865–4874.

Duncan, R., and Hershey, J.W. (1983). Identification and quantitation of levels of protein synthesis initiation factors in crude HeLa cell lysates by two-dimensional polyacrylamide gel electrophoresis. J. Biol. Chem. *258*, 7228–7235.

Eddy, S.R. (2004). Where did the BLOSUM62 alignment score matrix come from? Nat. Biotechnol. *22*, 1035–1036.

Frank, F., Virgili, G., Sonenberg, N., and Nagar, B. (2010). Crystallization and preliminary X-ray diffraction analysis of the MIF4G domain of DAP5. Acta Crystallogr. Sect. F Struct. Biol. Cryst. Commun. *66*, 15–19.

Furic, L., Rong, L., Larsson, O., Koumakpayi, I.H., Yoshida, K., Brueschke, A., Petroulakis, E., Robichaud, N., Pollak, M., Gaboury, L.A., et al. (2010). eIF4E phosphorylation promotes tumorigenesis and is associated with prostate cancer progression. Proc. Natl. Acad. Sci. USA *107*, 14134–14139.

Henis-Korenblit, S., Strumpf, N.L., Goldstaub, D., and Kimchi, A. (2000). A novel form of DAP5 protein accumulates in apoptotic cells as a result of caspase cleavage and internal ribosome entry site-mediated translation. Mol. Cell. Biol. *20*, 496–506.

Henis-Korenblit, S., Shani, G., Sines, T., Marash, L., Shohat, G., and Kimchi, A. (2002). The caspase-cleaved DAP5 protein supports internal ribosome entry site-mediated translation of death proteins. Proc. Natl. Acad. Sci. USA *99*, 5400–5405.

Holcik, M., and Sonenberg, N. (2005). Translational control in stress and apoptosis. Nat. Rev. Mol. Cell Biol. *6*, 318–327.

Holm, L., and Rosenström, P. (2010). Dali server: conservation mapping in 3D. Nucleic Acids Res. *38*(Web Server issue), W545–W549.

Hundsdoerfer, P., Thoma, C., and Hentze, M.W. (2005). Eukaryotic translation initiation factor 4GI and p97 promote cellular internal ribosome entry sequence-driven translation. Proc. Natl. Acad. Sci. USA *102*, 13421–13426.

Imataka, H., and Sonenberg, N. (1997). Human eukaryotic translation initiation factor 4G (eIF4G) possesses two separate and independent binding sites for eIF4A. Mol. Cell. Biol. *17*, 6940–6947.

Imataka, H., Olsen, H.S., and Sonenberg, N. (1997). A new translational regulator with homology to eukaryotic translation initiation factor 4G. EMBO J. *16*, 817–825.

Kim, C.Y., Takahashi, K., Nguyen, T.B., Roberts, J.K., and Webster, C. (1999). Identification of a nucleic acid binding domain in eukaryotic initiation factor eIFiso4G from wheat. J. Biol. Chem. *274*, 10603–10608.

Korneeva, N.L., First, E.A., Benoit, C.A., and Rhoads, R.E. (2005). Interaction between the NH2-terminal domain of eIF4A and the central domain of eIF4G modulates RNA-stimulated ATPase activity. J. Biol. Chem. *280*, 1872–1881.

Lee, S.H., and McCormick, F. (2006). p97/DAP5 is a ribosome-associated factor that facilitates protein synthesis and cell proliferation by modulating the synthesis of cell cycle proteins. EMBO J. *25*, 4008–4019.

Levy-Strumpf, N., Deiss, L.P., Berissi, H., and Kimchi, A. (1997). DAP-5, a novel homolog of eukaryotic translation initiation factor 4G isolated as a putative modulator of gamma interferon-induced programmed cell death. Mol. Cell. Biol. *17*, 1615–1625.

Lewis, S.M., Cerquozzi, S., Graber, T.E., Ungureanu, N.H., Andrews, M., and Holcik, M. (2008). The eIF4G homolog DAP5/p97 supports the translation of select mRNAs during endoplasmic reticulum stress. Nucleic Acids Res. *36*, 168–178.

Liberman, N., Marash, L., and Kimchi, A. (2009). The translation initiation factor DAP5 is a regulator of cell survival during mitosis. Cell Cycle *8*, 204–209.

Lomakin, I.B., Hellen, C.U., and Pestova, T.V. (2000). Physical association of eukaryotic initiation factor 4G (eIF4G) with eIF4A strongly enhances binding of eIF4G to the internal ribosomal entry site of encephalomyocarditis virus and is required for internal initiation of translation. Mol. Cell. Biol. *20*, 6019–6029.

Marash, L., Liberman, N., Henis-Korenblit, S., Sivan, G., Reem, E., Elroy-Stein, O., and Kimchi, A. (2008). DAP5 promotes cap-independent translation of Bcl-2 and CDK1 to facilitate cell survival during mitosis. Mol. Cell *30*, 447–459.

Marcotrigiano, J., Lomakin, I.B., Sonenberg, N., Pestova, T.V., Hellen, C.U., and Burley, S.K. (2001). A conserved HEAT domain within eIF4G directs assembly of the translation initiation machinery. Mol. Cell *7*, 193–203.

Morino, S., Imataka, H., Svitkin, Y.V., Pestova, T.V., and Sonenberg, N. (2000). Eukaryotic translation initiation factor 4E (eIF4E) binding site and the middle one-third of eIF4GI constitute the core domain for cap-dependent translation, and the C-terminal one-third functions as a modulatory region. Mol. Cell. Biol. *20*, 468–477.

Mossessova, E., and Lima, C.D. (2000). Ulp1-SUMO crystal structure and genetic analysis reveal conserved interactions and a regulatory element essential for cell growth in yeast. Mol. Cell *5*, 865–876.

Nevins, T.A., Harder, Z.M., Korneluk, R.G., and Holcík, M. (2003). Distinct regulation of internal ribosome entry site-mediated translation following cellular stress is mediated by apoptotic fragments of eIF4G translation initiation factor family members eIF4GI and p97/DAP5/NAT1. J. Biol. Chem. *278*, 3572–3579.

Özeş, A.R., Feoktistova, K., Avanzino, B.C., and Fraser, C.S. (2011). Duplex unwinding and ATPase activities of the DEAD-box helicase eIF4A are coupled by eIF4G and eIF4B. J. Mol. Biol. *412*, 674–687.

Pestova, T.V., Shatsky, I.N., and Hellen, C.U. (1996). Functional dissection of eukaryotic initiation factor 4F: the 4A subunit and the central domain of the

4G subunit are sufficient to mediate internal entry of 43S preinitiation complexes. Mol. Cell. Biol. *16*, 6870–6878.

Ponting, C.P. (2000). Novel eIF4G domain homologues linking mRNA translation with nonsense-mediated mRNA decay. Trends Biochem. Sci. *25*, 423–426.

Prévôt, D., Darlix, J.-L., and Ohlmann, T. (2003). Conducting the initiation of protein synthesis: the role of eIF4G. Biol. Cell *95*, 141–156.

Read, R.J. (2001). Pushing the boundaries of molecular replacement with maximum likelihood. Acta Crystallogr. D Biol. Crystallogr. *57*, 1373–1382.

Rogers, G.W., Jr., Richter, N.J., Lima, W.F., and Merrick, W.C. (2001). Modulation of the helicase activity of eIF4A by eIF4B, eIF4H, and eIF4F. J. Biol. Chem. *276*, 30914–30922.

Schütz, P., Bumann, M., Oberholzer, A.E., Bieniossek, C., Trachsel, H., Altmann, M., and Baumann, U. (2008). Crystal structure of the yeast eIF4A-eIF4G complex: an RNA-helicase controlled by protein-protein interactions. Proc. Natl. Acad. Sci. USA *105*, 9564–9569.

Shaughnessy, J.D., Jr., Jenkins, N.A., and Copeland, N.G. (1997). cDNA cloning, expression analysis, and chromosomal localization of a gene with high homology to wheat eIF-(iso)4F and mammalian eIF-4G. Genomics *39*, 192–197.

Sonenberg, N., and Hinnebusch, A.G. (2009). Regulation of translation initiation in eukaryotes: mechanisms and biological targets. Cell *136*, 731–745.

Studier, F.W. (2005). Protein production by auto-induction in high density shaking cultures. Protein Expr. Purif. *41*, 207–234.

Svitkin, Y.V., Gradi, A., Imataka, H., Morino, S., and Sonenberg, N. (1999). Eukaryotic initiation factor 4GII (eIF4GII), but not eIF4GI, cleavage correlates with inhibition of host cell protein synthesis after human rhinovirus infection. J. Virol. *73*, 3467–3472.

Warnakulasuriyarachchi, D., Cerquozzi, S., Cheung, H.H., and Holcík, M. (2004). Translational induction of the inhibitor of apoptosis protein HIAP2 during endoplasmic reticulum stress attenuates cell death and is mediated via an inducible internal ribosome entry site element. J. Biol. Chem. *279*, 17148–17157.

Yamanaka, S., Poksay, K.S., Arnold, K.S., and Innerarity, T.L. (1997). A novel translational repressor mRNA is edited extensively in livers containing tumors caused by the transgene expression of the apoB mRNA-editing enzyme. Genes Dev. *11*, 321–333.

Yamanaka, S., Zhang, X.Y., Maeda, M., Miura, K., Wang, S., Farese, R.V., Jr., Iwao, H., and Innerarity, T.L. (2000). Essential role of NAT1/p97/DAP5 in embryonic differentiation and the retinoic acid pathway. EMBO J. *19*, 5533–5541.